POLITECNICO DI TORINO
Repository ISTITUZIONALE

Geochemical characterization of a marine sediment core from the Joides Basin, Ross Sea, Antarctica

(Article begins on next page)

10 April 2024

Geochemical **characterization** of a marine sediment **core** from Terra Nova Bay, **Ross Sea,** Antarctica

F. Burgay[1,2]*, O. Abollino[3], S. Buoso[4], E. Costa[5], A. Giacomino[3], C. La Gioia[4], S. Fraterrigo Garofalo[6], G. Pecoraro[7], M. Malandrino[4]

[1] Institute of Polar Sciences – National Research Council – Via Torino 155, Venezia Mestre

[2] Ca' Foscari University of Venice – Department of Environmental Science, Informatics and Statistics – Via Torino 155, Venezia Mestre

[3] Department of Drug Science and Technology, University of Torino, Via Giuria 9, Torino, Italy

[4] Department of Chemistry, University of Torino, Via Giuria 5, Torino, Italy

[5] Department of Earth Sciences, University of Torino, Via Valperga Caluso 35, Torino, Italy

[6] Department of Applied Science and Technology, Polytechnic University of Turin, Corso Duca degli Abruzzi, 24, Torino, Italy

[7] Sea Marconi Technologies, Via Ungheria 20, Torino, Italy

* → Corresponding author francois.burgay@unive.it

Abstract

The chemical fractionation of ten metals (Al, Ti, Cr, Fe, Cd, Cu, Mn, Pb, Zn and Ni) is reported for a marine sediment collected offshore in the Terra Nova Bay, Ross Sea, Antarctica. To evaluate their mobility and availability, the BCR sequential extraction procedure was applied on 11 sections of the sediment. The analyses, performed both by ICP-OES and GF-AAS, highlighted that most of the elements were in the residual phase, showing a strong binding with the matrix and a low availability. The BCR sequential procedure allowed us to have an insight into the chemical properties of the sediment and provided useful information about the redox state of the sediment itself and important indication on the availability and partitioning of different metals. A chemometric treatment was

24 applied on the dataset and it showed a separation between the superficial and the lowest sections of
25 the core, the first being more influenced by the presence of Mn and the second by an increase in Al,
26 Ti, Fe, Cr and Pb concentrations.

27 **Keywords:** Antarctica, Ross Sea, marine sediment, sequential extraction procedure, sediment
28 diagenesis

29 **1. Introduction**

30   The Southern Ocean is the fourth largest ocean of the world. From the biological point of
31 view, it is a so-called High-Nutrient Low-Chlorophyll (HNLC) region. In other words, it is
32 characterized by a high concentration of nutrients, such as nitrates and phosphates, but it shows a
33 very low productivity (Martin and Fitzwater, 1988; Martin et al., 1990). The main reason, as
34 highlighted by Martin in 1990, is that this environment is Fe-limited. Through artificial (Smetacek et
35 al., 2012) and natural (Duprat et al., 2016) Fe fertilization, it has been shown that the productivity
36 increased with a significant atmospheric CO_2 drawdown to the surface ocean. Considering that one
37 of the main Fe source to the ocean is the Aeolian mineral dust (Jickells et al., 2005), during the coldest
38 and dustiest glacial periods, the increase in Fe supply caused an enhancement of the marine
39 productivity in the Subantarctic zone of the Southern Ocean (Martínez-Garcia et al., 2011) that likely
40 contributed to part of the total 100 ppm decrease in atmospheric CO_2 from the interglacial periods
41 (Lambert et al., 2015).

42   The Ross Sea, which is the southernmost sea on Earth, is comprised between Victoria Land
43 and Marie Byrd Land. It shows high marine productivity that contributes to at least half the annual
44 biological production of the entire Antarctic continental shelf (48 Tg C yr^{-1}) (Arrigo and Van Dijken,
45 2003). Nowadays, the primary production has a peak during the austral spring and, according to
46 satellite observations, can rise up to 4 g C m^{-3} d^{-1} (Rhodes et al., 2009). The productivity in the Ross
47 Sea has been associated to the availability of Fe and it was found that algal community growth can

48 be limited by iron deficiency in much of the Southern Ross Sea during summer, excluding the areas

49 where punctual iron sources exist (Sedwick et al., 2000). Taking advantage of the general absence

50 of pollution (Caroli et al., 2001), the Ross Sea is a privileged spot where performing biogeochemical

51 studies. On this purpose, marine sediment cores represent a unique archive to reconstruct the past

52 seawater composition. The low-sedimentation rate that characterizes the off-shore regions of polar

53 oceans (centimetres per thousand years) provides low-resolution records that can cover up to the last

54 millions of years of the Earth history (Martínez-Garcia et al., 2011). The knowledge of their

55 composition and of the involved sedimentation processes (i.e. biogenic, lithogenic and chemical

56 processes) can be extremely helpful to address several environmental and climatic questions. For

57 instance, through the determination of trace metals, it is possible to gain insight into the geochemical

58 and environmental processes that took place in the water column or into the diagenetic processes that

59 took place in the sediments themselves (Froelich et al., 1979).

60   Depending on how chemicals are bounded and on any pH or redox potential changes, sea

61 sediments can act not only as a sink, but also as a new sources of trace metals and pollutants (Ianni

62 et al., 2010). Therefore, to assess the environmental quality of a sediment core and to evaluate the

63 more available fractions, it is crucial to perform fractionation studies using sequential extraction

64 procedures. These methods are based on the use of a series of reagents chosen to solubilise in

65 sequence different fractions thought to be responsible for retaining the trace metals (Gleyzes et al.,

66 2002). The outcomes of sequential extraction procedures must be interpreted with caution because

67 the reagents are not very selective and metal re-adsorption and redistribution may take place after

68 each step. Nevertheless, such procedures provide useful information on metal binding mode and the

69 possible presence of anthropogenic contamination (Bacon and Davidson, 2008). One of the most

70 widespread sequential extraction procedures is the Tessier protocol (Tessier et al., 1979), that

71 partitions the elements into five operationally-defined geochemical fractions including: exchangeable

72 fraction; carbonate-bound fraction (acid-soluble); bound to Fe and Mn oxides fraction (reducible);

73 bound to the organic matter fraction (oxidable) and residual fraction. However, considering the

74 diversity of existing procedures and the lack of uniformity among the different methods, a

75 standardized three-step procedure was proposed by the former Community Bureau of Reference

76 (BCR), now the Standards, Measurements and Testing Programme (Quevauviller, 1998). It involves

77 three extractions steps with reagents of different strength in order to have information on the

78 exchangeable, water- and acid-soluble (first step), reducible (second step) and oxidizable (third step)

79 fractions. A comparison between the Tessier and the BCR protocol was performed on a Ross Sea

80 sediment core. It highlighted higher extraction percentages for the Tessier procedure, mainly because

81 of the stronger reagents and more drastic conditions (Casalino et al., 2013). In any case, considering

82 the availability of a certified reference material, shorter extraction times, an easier sample handling

83 and a detailed protocol, the adoption of the BCR procedure is preferable, especially if a comparison

84 among different sites is subsequently performed. Nevertheless, the Tessier protocol can be

85 advantageous when a distinction between a mobile and mobilizable fraction is object of studies

86 (Casalino et al., 2013).

87 This paper reports the results of a geochemical investigation performed on one sediment core

88 collected in Terra Nova Bay, Ross Sea, Antarctica, for ten metals: Al, Ti, Cr, Cd, Cu, Mn, Fe, Pb, Zn

89 and Ni. We reconstructed both their total concentration and their partitioning in the different fractions

90 according to the BCR procedure providing an insight on the diagenetic processes that might have

91 taken place in the sediment itself. An X-Ray Diffraction (XRD) investigation to understand if the

92 lithology of the sediment has changed over time is also reported.

93 **2. Regional setting**

94 The sediment core, coded sediment B, was sampled during the XX Italian Antarctic Survey

95 in 2004-2005 at the mooring B (73°59.7' S, 175°0.8' E) in an offshore area of the Ross Sea. The

96 collected sediment was located in the northern part of the Joides Basin at 588 meters depth (Figure

97 1). According to recent surveys performed at this location, the sinking particles are constituted mainly

98 by lithogenic (40-62% of the composition of particles in the near-bottom trap) and biogenic materials

99 (29-47% of the bulk dry material in the near-bottom trap) (Langone et al., 2000). Their composition

100 is strongly linked to the seasonal sea-ice cover: the lowest fluxes of biogenic silica were recorded

101 during austral autumn and winter, when the sea-ice extent was at its maximum (Langone et al., 2000;

102 Mezgec et al., 2017).

103 Ross Sea waters are generally oversaturated with respect to both calcite and aragonite,

104 showing a saturation state greater than 1 (Hauck et al., 2012; Rivaro et al., 2014). The occurence of

105 calcium carbonate species was well documented both in bottom traps (Bergami et al., 2009; Langone

106 et al., 2000) and in deep sediment cores (Casalino et al., 2013). However, the high productivity of the

107 Ross Sea and the respiration of the organic matter in the sediments can alter the sediment carbonate

108 chemistry, modifying their preservation (Hauck et al., 2012). The mean $CaCO_3$ content in the Ross

109 sea is 2% (714 g $CaCO_3$ m^{-2}) with the highest values (> 10%) being located in the Drygalsky Basin

110 (Domack et al., 1999).

111 Sediment B features were investigated in previous studies (Ravaioli et al., 1999) where it was

112 classified as siliceous mud. In particular, sediment B is constituted by olive-gray siliceous mud and

113 ooze without gravels. The sediment is characterized by a high concentration of biogenic silica (20 to

114 30% of the total sediment mass). The concentration of organic carbon, ranging from 0.86 to 1.23%,

115 does not show any clear trend along the core and it is the highest among all the investigated sediment

116 cores in the Ross Sea (Frignani et al., 2003; Langone et al., 2000; Ravaioli et al., 1999). Compared

117 to other sediment cores collected in different areas of the Ross Sea, sediment B is the one that shows

118 the highest concentration of macrobenthos species, especially polychaetes (up to the 75%). These

119 species, mainly located (80%) in the first 5 centimetres of the sediment, can provide potential

120 bioturbation of the sediment itself (Ravaioli et al., 1999).

121 The Ross Sea topography is shaped by glacial erosion and it is characterised by a complex

122 and heterogeneous morphology. This, results in a high variability in the sedimentation rates that can

123 change up to two-orders of magnitude within a distance of less than 600 km (DeMaster et al., 1992).

124   In the Joides Basin, the ^{14}C sedimentation rate ranges from 4.5 cm kyr^{-1} to 42 cm kyr^{-1} (DeMaster et

125   al., 1996; Langone et al., 1998; Mezgec et al., 2017; Salvi et al., 2004).

126   For sediment B, neither a ^{14}C dating nor a magnetic susceptibility profile were performed. For

127   this reason, we compared the sediment accumulation rates (SAR) from different sediment cores

128   collected close to sediment B (Figure 1; Table 1). Moreover, we observed that the diatomaceous mud

129   layer, representative of Holocene open water conditions, has the same thickness both in site B and in

130   site ANTA19-C14 (Corradi et al., 2003) which indicates similar sedimentation rates. In addition, site

131   ANTA19-C14 has a ^{14}C sediment accumulation rate (38.3 cm kyr^{-1}) similar to the one calculated for

132   sediment Y5 (38 cm kyr^{-1}), located less than 10 km away from site B. For these reasons, we assume

133   that sediment B should preserve a SAR similar to the one calculated for the nearby sediments which

134   ranges from 37 to 42 cm kyr^{-1}.

135   In this paper, we performed a comparison with other sea sediment cores collected in the Terra

136   Nova Bay, which were analysed using the BCR extraction procedure. These sediments, coded D and

137   H, were collected in a polynya area and on the outer continental shelf respectively (Casalino et al.,

138   2013; Malandrino et al., 2010). They are characterized by a lower biogenic silica concentration than

139   sediment B (1-4.5% and 5-8% respectively) and with low sediment accumulation rates of 1.7 cm kyr^{-}

140   ^{1} (Frignani et al., 2003). The organic content is higher in sediment H ($\approx$ 0.3%) than in sediment D ($\approx$

141   0.15%), with an enrichment at surface in both sites.

142   **3. Material and methods**

143   *3.1 Sample processing*

144   A stainless-steel box corer was used to sample 50 cm of sediment. The core was extruded

145   from the corer and subsampled in different sections using a knife with a Teflon blade (Table 2). To

146   avoid contamination from any metallic part, only the inner part of the core was collected and

147   transferred into polycarbonate Petri boxes, stored at -25 °C and shipped to the University of Turin

148 (Italy). Subsequently, all the sections were defrosted for 18 hours in previously cleaned polycarbonate

149 boxes under a Class-100 laminar flow hood located in a Class-100.000 clean room. They were dried

150 under a Class-100 laminar hood, homogenized at 320 rpm for 15' and then stored in polycarbonate

151 boxes. To take into account the moisture content, a sub-sample of sediment was dried at 105°C until

152 constant mass was attained. Moisture contents were used to calculate all sediment characteristics on

153 a dry mass basis.

154   We performed a sequential extraction procedure following the three-step Modified BCR

155 protocol (Rauret et al., 2000). We will refer to the three extracted phases as the labile, reducible and

156 oxidizable fractions respectively. All the bottles and vessels used during this process were previously

157 filled for 7 days with a 5% solution of 65% HNO_3 (Sigma Aldrich Merck, USA), then rinsed with

158 Ultrapure Water (UPW) and filled until their use with a 2% solution of 37% HCl (Sigma Aldrich

159 Merck, USA). All the acids were purified by sub-boiling distillation in a quartz still and UPW was

160 used throughout.

161   The labile fraction was extracted adding 20 ml of 0.11 M acetic acid (ACS Reagent,

162 Honeywell, USA) to 0.5 g of sample in a reaction vessel. The sample was shaken for 16h at room

163 temperature. The supernatant was then filtered and collected in previously cleaned polyethylene

164 bottles, acidified with 100 μl of 65% HNO_3 (Sigma Aldrich Merck, 65%) and made up to 50. The

165 residue was then washed with 10 ml of UPW.

166   The reducible fraction was extracted adding to the washed solid residual, 20 ml of a 0.1 M

167 hydroxylamine hydrochloride (ACS Reagent, Merck, DE) solution adjusted to pH 2. The sample was

168 shaken for 16h at room temperature. The supernatant was then filtered and collected in previously

169 cleaned polyethylene bottles, acidified with 100μl of 65% HNO_3 (Sigma Aldrich Merck, USA) made

170 up to 50 ml. The residue was then washed with 10 ml of UPW.

171   The oxidizable fraction was extracted adding to the washed solid residual, 5 ml of 33% H_2O_2

172   (Extrapure, Honeywell, USA) at room temperature for 1h. The solution was occasionally shaken.

173   Then, the uncovered reaction vessel was heated at 85°C using a water bath for 2h until the total

174   volume was reduced to 2 ml. 5 ml of 33% H_2O_2 were further added and kept for 1h at 85°C. Then the

175   vessel was uncovered again until the final volume of 0.5 ml was reached. At this point, 25 ml of 1 M

176   ammonium acetate (trace metal basis, Sigma Aldrich Merck, USA) (adjusted to pH 2 with 65%

177   HNO_3) were added and the covered vessel was shaken for 16h at room temperature. The supernatant

178   was then filtered and collected in previously cleaned polyethylene bottles, acidified with 100μl of

179   65% HNO_3 (Sigma Aldrich Merck, USA) and made up to 50 ml.

180   To have information on the total metal concentrations, an acid digestion in a Milestone MLS-

181   12000 MEGA Microwave was also performed. 100 mg of dried sample were treated with 5 ml of

182   *aqua regia* and 2 ml of hydrofluoric acid (48%, ACS Reagent, Sigma Aldrich Merck, USA) in PTFE

183   bombs. The applied digestion program was: 300s at 250 W, 300s at 400 W, 300s at 600 W, 300s at

184   250 W. A ventilation step of 25 minutes followed. 0.7 g of boric acid were added and the bombs

185   were further heated for 300s at 250 W and cooled again with a ventilation step of 15 minutes. The

186   final solution was filtered and made up to 50 ml with UPW.

187   All experiments were executed in triplicate and the same procedure was performed for the

188   blanks.

189   *3.2 Apparatus and reagents*

190   All the extracts were analysed either by ICP-OES (Varian Liberty 100 Inductively Coupled

191   Plasma-Optical Emission Spectrometer) equipped with a V-groove nebulizer or by GF-AAS (Perkin

192   Elmer 5100 Graphite Furnace Atomic Absorption Spectrometer) equipped with a heated graphite

193   atomizer and Zeeman-effect background correction, depending on the concentration of the analytes

194   in the samples and on the Limit of Detection (LoD) and Limit of Quantification (LoQ) (Table S2).

195 LoD, LoQ and more details on the instruments used for the determination of the different species are

196 reported in the following sections. Calibration curves were performed using the external standard

197 calibration method for all the ten elements of interest. Standards were prepared from single element

198 1000 mg L^{-1} stock solutions (Merck Titrisol).

199 X-ray powder diffraction (XRD) data were collected on specimens hand ground with an agate

200 mortar and mounted on a zero-background Si-monocrystal flat sample holder, using an automated

201 PW3050/60 PANalytical X'Pert-PRO diffractometer in Bragg-Bretano geometry with Ө-Ө setup,

202 ~~Real~~ Real-Time Multile Strip detector and Cu-Kα radiation. Data were analysed in the 3-70° 2Ө range

203 with the Diffrac Plus (2005) software (EVA 11,00,3).

4. Results

4.1 Quality assurance

206 The measurement trueness was evaluated both for the total digestion and for the sequential

207 extraction method. For the total digestion, the MURST-ISS-A1 (Antarctic sediment) reference

208 material (Caroli et al., 1998) was analysed using three replicates, while for the BCR protocol the

209 BCR-701 (Lake Sediment) reference material was analysed (Casalino et al., 2013) using three

210 replicates for each step. Regarding the total digestion of the sediment core and focusing on five main

211 elements, the average recovery was 86 ± 9% (Table 3). Relatively to the BCR sequential extraction

212 protocol, we found average recoveries of~~:~~ 81 ± 23 % for the first step, 91 ± 15% for the second step

213 and 79 ± 15% for the third one (Table 4). Overall, our results underestimated the real concentration

214 of some elements, in particular Zn (51%) in the first fraction and Cd (52%) in the third one. The

215 uncertainty associated to each concentration value is comparable to the ones found in other studies

216 (Cuong and Obbard, 2006).

217 The Limit of Detection (LoD) and the Limit of Quantification (LoQ) were determined through

218 the ICP-AES and GF-AAS analyses of the blanks (number of readings: 3). The returned average

219 values were then summed to three times (for the LoD) and ten times (for the LoQ) the standard

220 deviation of the blank measurements. The results are summarized in Table S1.

221 *4.2 Total metal concentration and sediment lithology*

222 Total metal concentrations in the core sections are reported in Table 5. Al, Fe and Ti are the

223 metals with the highest concentrations. This indicates that they are the main constituents of the

224 sediment lithology. The variability of each element along the core, expressed as relative standard

225 deviation (RSD%), did not exceed 15%, apart from Mn (47%) and Cd (60%). This suggests that the

226 lithology of the sediment did not significantly change within the studied period. Additional clues

227 come from the XRD analysis performed on selected samples (B01, B02, B12, B17, B22, B27, B32,

228 B37, B42, B45), which does not highlight any modification in the sediment composition (Figure S1).

229 The sediment is mainly constituted by quartz (SiO_2), plagioclase ($(Na,Ca)(Si,Al)_4O_8$), K-feldspar

230 ($KAlSi_3O_8$), mica $(Ca,Na)(Al,Mg,Fe)_{2,3}(Si,Al)_4O_{10}(OH)_2$ and halite (NaCl).

231 To quantify the carbonate concentration in the sediment we applied the Loss of Ignition

232 method, based on the combustion of 1 g of dried sediment at 950°C for 2 hours (Heiri et al., 2001).

233 More details on the analytical procedure and on the results are reported in the Supplementary Material

234 (Figure S5). The results show that the carbonate content of the sediment ranges from 2% to 5% of the

235 total dried mass reflecting the average calcium carbonate concentration retrieved from 52 sediments

236 collected in the Ross Sea (Hauck et al., 2012). In our record, we found a significantly amount of trace

237 elements associated to with the first BCR fraction. This fraction, as we will discuss deeply in the

238 following, extracts metals that can be associated with carbonates. For this reason, and according to

239 former interpretations of similar extraction results (Casalino et al., 2013; Ianni et al., 2010;

240 Malandrino et al 2010), we hypothesize the presence of carbonate minerals, such as otavite ($CdCO_3$),

241 rhodochrosite ($MnCO_3$) and siderite ($FeCO_3$) in our sediment core. Nevertheless, to better assess

242 their occurrence, more focused investigations need to be performed (e.g. through Scanning Electron

243 Microscope analyses).

244　　*4.3 Metal partitioning*

245　　　　　The results of the metal partitioning will be interpreted assuming the following features

246　　(Abollino et al., 2006; Reddy et al., 2001): a) the first fraction corresponds to loosely held metal ions,

247　　including the exchangeable and soluble forms, that can be readily extracted and are therefore

248　　potentially available for the biota. Metals associated with carbonates and easily soluble

249　　oxide/hydroxides in mildly acidic conditions are present in the first fraction as well; b) the second

250　　fraction is composed of additional metal oxides/hydroxides soluble at acidic pH and metals associated

251　　with Fe-Mn oxides; c) the third fraction comprises metal ions associated with easily oxidizable solids

252　　or compounds, including organic matter and sulphides.

253　　　　　Figures 2-4 summarize the distribution of the elements in the four fractions. All the

254　　concentration values for each fraction and section are reported in the Supplementary Material (Table

255　　S4, Table S5 and Table S6)

256　　　　　Iron, aluminium, titanium and chromium (Figure 2): these elements are mainly present in the

257　　residual phase ($> 80\%$) as silicates. This is consistent with the inert feature of these metals. Fe, despite

258　　its biological relevance, is also a key constituent of sedimentary rocks and it is mainly present in the

259　　sediment in its insoluble form (Gleyzes et al., 2002).

260　　　　　Zinc and copper (Figure 3): they are mainly extracted in the residual phase ($> 50\%$). However,

261　　they are also present in high concentration along the whole core in the second and third fraction. This

262　　trend suggests that these elements are scavenged by amorphous oxides (Casalino et al., 2013) and ca

263　　be associated with humic and fulvic acids (10% and 20% for Zn and Cu respectively) (Braguglia et

264　　al., 1995). Low extraction percentages (from 4 to 14% and from 2% to 4% for Zn and Cu respectively)

265　　are recorded in the first fraction.

266　　　　　Nickel (Figure 3): it is present in a significant amount into all the different fractions showing

267　　a heterogeneous behaviour.

268   Manganese (Figure 3): it shows a peculiar fractionation as a function of depth. In the upper

269   sections it is mainly extracted in the first and second fractions probably as rhodochrosite ($MnCO_3$)

270   and as oxide (33% and 34% respectively), while below 6.5 centimetres depth, it mainly occurs in the

271   residual phase.

272   Cadmium and lead (Figure 4): cadmium is mainly present in the acid-soluble phase ranging

273   from 0.03 to 0.262 mg kg^{-1} with maximum values between 20 and 30 cm depth. Acid-soluble Cd

274   constituted up to the 70% of the total Cd present in the sediment, while the remaining part is

275   associated to Fe-Mn oxides. Cd is not detected in the oxidizable fraction. Lead is mainly extracted in

276   the second and third fraction showing an opposite trend between these two fractions. In particular,

277   lead associated with Fe oxides become increasingly more relevant with depth (from 17% to 67%),

278   while a significant drop is observed in the oxidizable Pb fraction from 6 cm downwards (from 40%

279   to 10%).

280   **5. Discussion**

281   *5.1 Discussion on the total metal concentration*

282   To determine if any anthropogenic contamination or any extra source affects the chemical

283   composition of the sediment, we calculated the enrichment factors (EF) using the upper crustal

284   elemental abundances (Hans Wedepohl, 1995) such that EF = $([x]/c)_{sample}/([x]/c)_{upper\ crust}$ where c is

285   one of the conservative crustal elements (i.e. Ti for our aims) and x the element we wanted to

286   investigate (Table S3). Values higher than 10 indicate potential additional sources (e.g. pollution).

287   However, we did not appreciate any value greater than 10. This confirms that all the geochemical

288   evaluations that follow, are related to natural processes only.

289   Mn is more concentrated in the first 2 centimetres of the sediment, while its concentration

290   decreases below 3.5 centimetres to a lower and almost constant value. Comparing our results with

291   other studies performed in other locations of the Ross Sea (Casalino et al., 2013; Malandrino et al.,

292   2010), we found that sediment B represents a *unicum* concerning the total Mn behaviour. Both in site

293   H (Casalino et al., 2013) and in site D (Malandrino et al., 2010), the total Mn concentration was higher

294   (average: 1000 mg kg^{-1} and 544 mg kg^{-1} respectively) and with a lower variability along the core

295   (RSD: 8% and 15% respectively). We interpreted this difference between sediment B and sediment

296   D and H, as a consequence of different diagenetic processes related to the different sediment redox

297   conditions that will be discussed in the following.

298   In sediment B, the Cd concentration increases with depth from an average of 0.06 mg kg^{-1},

299   recorded in the first 3 cm, to a maximum of 0.4 mg kg^{-1} at 27 cm depth. The average concentration

300   along the whole core is 0.2 mg kg^{-1}, similar to the one recorded in site H (Casalino et al., 2013), but

301   lower than the one recorded in site D (Malandrino et al., 2010).

302   The lower crustal element (e.g. Al, Fe, Ti, Mn) concentration recorded at site B than at site D

303   and H can be linked to the higher SAR that characterizes this site. Considering that, at site D the

304   highest values for these elements are recorded in the deepest parts of the sediment, we hypothesize

305   that, accordingly to the available sediment accumulation rate and ^{14}C dating (Frignani et al., 2003;

306   Malandrino et al., 2010), this part corresponds to colder and dustier periods (e.g. Antarctic Cold

307   Reversal). Alternative explanations can rely on the higher exposure to continental weathering (e.g.

308   due to the strong katabatic winds) or on the faster degradation of the biological component than the

309   mineralogical one in the bottom part of the sediment (Malandrino et al., 2010). This hypothesis is

310   consistent with the progressive decrease in the total organic carbon concentration recorded in this

311   sediment as a function of depth (Frignani et al., 2003).

312   A Principal Component Analysis (PCA) and a Hierarchical Cluster Analysis (HCA) were

313   performed on the total element content (Figure 5). The PCA shows a clear correlation among Al, Ti,

314   Fe, Cr and Pb which constituted the lithological bulk of the sediment, while the HCA shows a

315   separation among the samples as a function of depth: 1) B01 and B02 forms one distinct group, mainly

316   influenced by the high concentration of Mn. According to with the presence of macrobenthos in the

317 upper sections of the core (Langone et al., 1998), ~~it is possible that the first centimetres ar~~the first

318 centimetres may be affected also by bioturbation processes; 2) from B07 to B22; 3) the sections from

319 B27 to B37 are mainly influenced by Cu, Cd, Zn and Ni; 4) B42 and B45 are characterized by an

320 increase in crustal elements such as Al, Ti, Fe, Cr and Pb. Contrarily to what described for sediment

321 D, in this context, we exclude that this increase in the crustal element concentration can be linked to

322 an increase in the organic matter degradation. Indeed, the organic matter concentration appears to be

323 constant throughout the entire sediment (Ravaioli et al., 1999). This increase can be likely associated

324 to external inputs that are difficult to identify in the absence of an absolute dating of the core.

325   We compared the average total concentrations of the elements in sediment B with the ones

326 retrieved from other sites in the Terra Nova Bay (Table 6). The higher concentrations of Al and Fe

327 in site D than in site B and H suggest that site D is more exposed to continental weathering.

328 Furthermore, site D shows higher Cd concentration than sediment H and B. However, how we will

329 discuss in the metal partitioning section, this increase is likely due to a stronger terrigenous input that

330 characterizes the polynya than the other two sites. Site H and Site B show similar trace metals

331 concentration ranges, likely because they are both located offshore.

332 *5.2 Discussion on the metal partitioning*

333   The distribution of manganese in marine sediments provides useful information on the

334 sediment oxidation potentials (Pedersen and Price, 1982). In some circumstances, the presence of

335 Mn(II)-carbonate is also considered a proxy for short oxygenation events in regions where anoxic

336 conditions prevail (Lenz et al., 2014). Under these conditions, Mn, present in its reduced and soluble

337 form (Mn^{2+}), is leached from the sediment and enriched in the anoxic stratified bottom waters. In case

338 of short-term oxygenation events, soluble Mn^{2+} can be oxidized back to Mn-oxide. When the anoxic

339 conditions are restored, it is reduced back to Mn(II) and, thanks to the alkalinity increase promoted

340 by sulphur reducing bacteria, it can precipitate as rhodochrosite. These events are clearly visible in

341 the sediment core stratigraphies as thin rhodochrosite layers (Huckriede and Meischner, 1996).

342   Mn species are also involved in the diagenesis of marine organic matter together with nitrate,

343   Fe, and sulphate. Under semi-anoxic conditions, the organic carbon is oxidized by Mn(IV), which

344   releases soluble Mn^{2+} to the porewater. Mn^{2+} can diffuse upwards in layers where more oxic

345   conditions prevail and it can accumulate as MnO_2 (Froelich et al., 1979). This process provides a

346   mechanism for stripping manganese from the deepest and anoxic sections of the sediment,

347   accumulating and redepositing Mn oxides at the sediment-water interphase.

348   The adoption of the BCR protocol allowed us to investigate both the acid-leachable phase of

349   Mn, where it is likely present as rhodochrosite (I fraction), and the reducible fraction, where it is

350   present as oxide (II fraction). Our record shows that manganese extracted in the first fraction exhibits

351   a maximum at 1 cm depth (40% of the total Mn, which corresponds to 201 mg kg^{-1}) followed by a

352   decrease to the 3% of the total Mn concentration (4.6 mg kg^{-1}) from 8 cm depth to the bottom (Figure

353   3, Table S4). Mn-oxide concentration decreases sharply from 35% of the total Mn concentration (193

354   mg kg^{-1}) at the surface, to 10% at 6 cm depth (21 mg kg^{-1}, Figure 3, Table S5). This is consistent with

355   what postulated by Froelich et al., (1979), which described an enrichment of Mn species at the

356   sediment-water interphase and a subsequent pauperization of Mn-oxides in the anoxic part of the

357   sediment. Thus, the Mn-oxide enrichment recorded at the surface can be explained as the re-oxidation

358   of Mn^{2+}, which has migrated upwards from the anoxic section of the sediment through the sediment

359   porewaters (Froelich et al., 1979).

360   The presence of a high concentration of labile-Mn, together with the high concentration of

361   Mn-oxides at the water-sediment interphase, suggests that part of the Mn-oxides can be reduced by

362   the respiration of the organic matter. Alternatively, a fraction of the total Mn^{2+} that diffuses upwards

363   can precipitate as rhodochrosite instead of being oxidized by the O_2 excess. Lastly, the role of

364   bioturbation in influencing the distribution of the Mn solid phase cannot be excluded *a priori,*

365   considering the presence of different ~~macroozobenthos~~ macrozoobenthos species localized in the first

366   5 cm of the core (Ravaioli et al., 1999).

367   The interpretation of the Mn species distribution is consistent with the behaviour of the Fe

368   species. Indeed, Fe is involved in the respiration of the organic matter under stronger anaerobic

369   conditions (Wersin et al., 1991). In sediment B, we observed that, in the uppermost 3.5 cm, Fe

370   extracted in the II fraction, builds up the 10-12% (from 1500 to 2500 mg kg^{-1}) of the total Fe. Below

371   this horizon, the concentration of Fe oxides decreased down to the 4% ($\approx$740-1000 mg kg^{-1}) of the

372   total Fe (Table S4, Figure 2). This suggests that Fe(III) has been dissolved into soluble Fe(II) species

373   accordingly to a plausible increase in the sediment anoxicity with depth. This interpretation is

374   endorsed by the increase in the oxidizable Fe fraction with depth. Contrarily to what observed for the

375   Mn species, the recycling of Fe upwards is reduced because of its tendency to be more easily captured

376   by sulphide to form FeS species (Calvert and Pedersen, 1996).

377   Taking advantage from the availability of other two sediment cores in the Ross Sea (sediment

378   H and sediment D) on which a BCR extraction procedure was performed, we investigated the

379   differences in their redox states (Casalino et al., 2013; Malandrino et al., 2010). Neither sediment H

380   nor sediment D show a significant variability in the Mn-oxides fraction that ranges from 3-7% and 2-

381   6% of the total Mn concentration respectively. However, in sediment H the concentration of Mn-

382   oxides is one order of magnitude higher (554 $\pm$ 134 mg kg^{-1}, 70% of total Mn) than in sediment D

383   (25 $\pm$ 6 mg kg^{-1}). This, together with the absence of any enrichment in labile Mn along the whole

384   core, indicates an overall oxic condition at this location. To the contrary, an increase in labile-Mn, is

385   observed in the uppermost 3 cm of sediment D (15-6% vs 1% at the bottom). This layer, in the

386   absence of a Mn-oxide enrichment, might indicate anoxic conditions of the site D bottom waters.

387   Organic complexes dominate the total concentration of Fe, Zn and Cu in seawater (Morel and

388   Price, 2003). This behaviour is reflected in sediment B, where these metals, and especially Zn and

389   Cu, are extracted in significant concentrations in the third fraction. In particular, these species exhibit

390   an enrichment at intermediate depths (20-25 cm) where their concentration in the oxidizable fraction

391   rise up to the 11% (for Zn), 26% (Cu) and 5% (Fe). Even if for Fe, a significant contribution can

392 come from the FeS species formed as a consequence of the respiration of the organic matter under

393 anaerobic conditions, Zn and Cu are strongly bound to the organic matter as shown in another study

394 performed close to site B (Calace et al., 2005). This can reflect the high productivity in this area,

395 which causes a greater amount of organic and biogenic remains to get buried (Ianni et al., 2010).

396   In seawater, Cd shows a nutrient-like behaviour. Moreover, having, in its hydrated form, a

397 similar ionic radius to that of the Ca ion, it can be taken up through the Ca-ion pumps by several

398 marine organisms (Merian et al., 2004). This, can result in an enrichment in the biogenic calcareous

399 debris (Ciaralli et al., 1998; Ianni et al., 2010).The PCA performed on the first fraction (Figure S2)

400 showed that Cd influences mainly the bottom sections of the core.

401   Comparing sediment B with sediment D, we observed that sediment D has a significantly

402 lower average concentration of Cd associated to the first fraction, with the average value of 5.4 ± 4.8

403 %, but a higher total Cd content (up to 1.17 mg kg^{-1}). Considering that site D is a coastal site, this

404 higher content in total Cd concentration can derive from a stronger terrigenous input (Malandrino et

405 al., 2010). The lower concentration obtained in the first fraction might indicate a lower uptake from

406 the marine phytoplankton at this location. This is consistent with the higher productivity recorded in

407 site B than in site D (Frignani et al., 2003; Langone et al., 2000), that might have led to different Cd

408 biological uptakes.

409   Accordingly with previous studies, we found that Mn and, especially, Fe oxides are good Pb

410 scavengers (Ianni et al., 2010) since the largest fraction of Pb is associated with the II fraction. This

411 is true in particular below 3.5 cm depth, where its concentration increased up to the 68% of the total

412 Pb. It is also well known that the organically complexed lead fraction in seawater can constitute a

413 significant portion of the total Pb (Capodaglio et al., 1998). In sediment B, a high amount of Pb is

414 extracted in the oxidizable fraction (25-40%) in the uppermost 3.5 cm of the sediment. Considering

415 the redox state of the sediment discussed above, we assume that Pb is bound to the organic matter

416 rather than present as PbS. The increase in this fraction can be explained by the low concentration of

other micronutrients, which might have led to an increase in the Pb organic complexation in the water column. However, below 3.5 cm depth, the oxidizable Pb fraction decreased down to 8-10% of the total Pb. This is mirrored by an increase in the Zn and Cu extracted in the third fraction, which suggests an higher affinity of these micronutrients to the organic matter and produces a decrease in the concentration of organically bounded Pb, in favour of an increase in Pb scavenged by Fe-oxides (II fraction).

6. Conclusions

In this study, we showed the geochemical features of a sediment core collected in the Terra Nova Bay (Antarctica). Through a mineralogical study, we evaluated the lithology of the sediment and we found that it was mainly constituted by felsic rocks and it did not significantly change along the whole core. Most of the elements were present in the residual phase, indicating a strong binding with the sediment matrix and a low availability.

The BCR protocol allowed us to investigate in details the geochemical properties of the sediment highlighting several sediment diagenetic processes due to the respiration of the organic matter. Furthermore, we were able to understand which elements were bounded to the organic matter and which was their behaviour accordingly with their abundance and availability in the water column. Lastly, we discussed the role of Cd, which was mainly extracted in the first fraction. Because of the high organic carbon flux recorded at sediment B, we propose that the observed enrichment in labile Cd was mainly due to a non-selective biological uptake.

7. Data availability

All data are available upon request to the authors

Aknowledgments

442 **Tables and figures**

443 **Table 1** – Locations and sediment accumulation rates for sediments collected in the same area of
444 sediment B.

445

Core	Coordinates	Sediment Accumulation Rate	References
Site B (red dot)	73°59.7'S; 175°0.8' E	n.a.	*This work*
ANTA91-14 (violet dot)	73°52.4' S; 175°24.8' E	38.3 cm kyr^{-1}	(Frignani et al., 1998)
Y5 (green dot)	74°00.0' S; 174°44.0' E	38 cm kyr^{-1}	(Calace et al., 2004)
WRS_JB (blue dot)	73°49.0' S; 174°39.0' E	42 cm kyr^{-1}	(Mezgec et al., 2017)
Site D (black dot)	75°06.0' S; 164°13.0' E	1.7 cm kyr^{-1}	(Malandrino et al., 2010)
Site H (yellow dot)	75°56.0' S; 177°36.0' W	1.7 cm kyr^{-1}	(Casalino et al., 2013)

446

447

448

449

450

451

452

453 **Table 2** – Sections of the sediment and associated depth

Section	Depth /cm
B01	0-0.5
B02	0.5-1
B07	3-3.5
B12	5.5-6
B17	8.0-8.5
B22	11-12
B27	16-17
B32	21-22
B37	26-27
B42	32-34
B45	38-40

454

455 **Table 3** – Cu, Cr, Zn, Mn and Mn recovery from the standard reference material MURST-ISS-A1.

456 All values are reported in mg kg^{-1}.

	Analysed CRM value	Certified CRM value	Recovery %
Cu	5.15 ± 0.09	5.79 ± 1.59	89 %
Cr	30.8 ± 0.8	42.1 ± 3.4	71%
Zn	45.5 ± 0.1	53.3 ± 2.7	85%
Mn	420 ± 12	446 ± 19	94%
Fe	2.25 ± 0.07	2.44 ± 0.07	92%

457

458

459

460 **Table 4 –** Results of analysis of standard reference material BCR-701 in comparison with certified

461 values for the different step of the BCR Protocol. All values are reported in mg kg^{-1}.

	Analyzed CRM value	Certified CRM value	Recovery %
Step 1			
Cd	5.7 ± 0.6	7.3 ± 0.4	78%
Cr	2.16 ± 0.05	2.3 ± 0.2	94%
Cu	57.7 ± 0.3	49.3 ± 1.7	117%
Ni	12.4 ± 0.4	15.4 ± 0.9	81%
Pb	1.97 ± 0.08	3.2± 0.2	62%
Zn	104 ± 8	205 ± 6	51%
Step 2			
Cd	4.18 ± 0.02	3.8 ± 0.3	110%
Cr	41.3 ± 0.3	46 ± 2	90%
Cu	82 ± 1	124 ± 3	66%
Ni	25.6 ± 0.7	27 ± 1	95%
Pb	108.0 ± 0.1	126 ± 3	86%
Zn	112 ± 2	114 ± 5	98%
Step 3			
Cd	0.14 ± 0.03	0.27 ± 0.06	52%
Cr	121 ± 5	143 ± 7	85%
Cu	38 ± 2	55 ± 4	69%
Ni	14.0 ± 0.6	15.3 ± 0.9	92%
Pb	7.4 ± 0.3	9 ± 2	82%
Zn	42 ± 1	46 ± 4	91%

462

463

Depth /cm	Cr	Mn	Zn	Ti	Cu	Al	Fe	Cd	Pb	Ni
-0.5	39.3 ± 0.6	624 ± 5	94.1 ± 0.5	2560 ± 20	29.5 ± 0.5	37000 ± 4000	24000 ± 2000	0.10 ± 0.01	9.0 ± 0.3	19.9 ± 0.4
-1	39.5 ± 0.4	544 ± 9	89 ± 1	2560 ± 20	29.4 ± 0.3	34000 ± 3000	22000 ± 1000	0.06 ± 0.02	8.7 ± 0.4	18.4 ± 0.2
-3.5	40.7 ± 0.5	321 ± 7	89.8 ± 0.6	2680 ± 40	29.0 ± 0.9	33500 ± 100	23500 ± 200	0.04 ± 0.01	9.1 ± 0.4	16.8 ± 0.3
-6	40.6 ± 0.4	248 ± 6	88 ± 2	2570 ± 20	30 ± 1	36000 ± 2000	23000 ± 1000	0.12 ± 0.01	11.6 ± 0.3	17.1 ± 0.8
-8.5	42 ± 1	226 ± 4	87 ± 1	2600 ± 20	31.1 ± 0.5	35000 ± 2000	21000 ± 1000	0.24 ± 0.02	11.4 ± 0.3	22 ± 5
-11	39.3 ± 0.2	210 ± 4	82 ± 2	2500 ± 40	34.4 ± 0.9	37000 ± 6000	22000 ± 2000	0.25 ± 0.01	10.6 ± 0.5	18 ± 1
-17	38.5 ± 0.3	204 ± 3	94 ± 2	2420 ± 40	33.3 ± 0.9	33000 ± 2000	19600 ± 900	0.48 ± 0.02	7.7 ± 0.2	19.9 ± 0.1
-22	40.4 ± 0.5	210 ± 2	100.4 ± 0.2	2530 ± 50	35 ± 1	35000 ± 2000	22000 ± 2000	0.37 ± 0.01	8.4 ± 0.1	21.2 ± 0.3
-27	43 ± 1	237 ± 6	109 ± 3	2780 ± 90	31.3 ± 0.2	36000 ± 1000	24000 ± 1000	0.37 ± 0.01	10.2 ± 0.3	22.9 ± 0.6
-34	47.1 ± 0.6	274 ± 3	110 ± 2	3070 ± 60	27.4 ± 0.7	45000 ± 6000	28000 ± 3000	0.28 ± 0.02	11.2 ± 0.7	23.7 ± 0.6
-40	45 ± 3	270 ± 20	95 ± 8	3000 ± 200	24 ± 1	43000 ± 7000	25000 ± 4000	0.37 ± 0.04	12 ± 1	20 ± 2
AV	41.3	306.1	94.4	2651.8	30.4	36772	23100	0.2	10	19.9
MAX	47.1	623.7	110.1	3069.8	34.7	45000	28000	0.5	12.2	23.7
MIN	38.5	204.4	81.5	2420.0	24.2	33000	19600	0.04	7.7	16.8
DEV	6	47	10	8	10	10	10	60	15	12

Table 5 – Total metal content. All concentrations are expressed in mg/kg. AV = average concentration. MAX = maximum concentration. MIN = minimum concentration. DEV = standard deviation (%)

466 **Table 6** - Concentration ranges found in the sediment H (Casalino et al., 2013), sediment D

467 (Malandrino et al., 2010) and sediment B (this work). Values are in mg kg^{-1}.

468

469

Element	Site D	Site H	**Site B**
Al	42 700-62 340	35 310-53 040	**33 000-45 000**
Cd	0.49-1.17	0.23-0.86	**0.04-0.5**
Cr	12-63	33-51	**39-47**
Cu	21-116	32-66	**24-35**
Fe	18 960-41 120	19 043-33 475	**19 600-28 000**
Mn	425-714	849-1176	**204-624**
Ni	16-36	13-34	**17-24**
Pb	15-31	10-15	**8-12**
Ti	2 670-3440	1 858-3 327	**2 420-3 070**
Zn	75-109	74-114	**81.5-110**

470　**Figure 1** – Map of the Ross Sea. The red circle represents the sediment B (this study). The other

471　cores are also shown: Y5 (green dot), WRS-JB (blue dot) and ANTA91-14(violet dot) where used

472　for a better evaluation of the sediment accumulation rate. Site D (black dot) and site H (yellow dot)

473　where used to perform a comparison. *Credits:* Antarctic Mapping Tools for Matlab (Greene et al.,
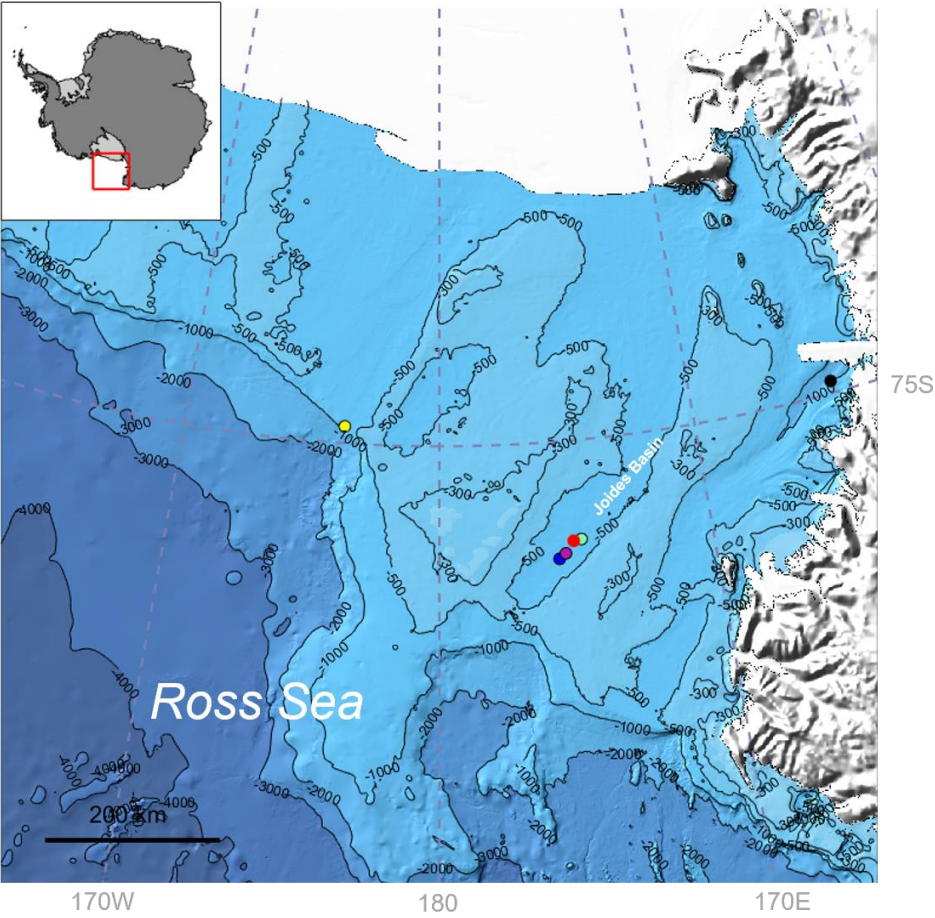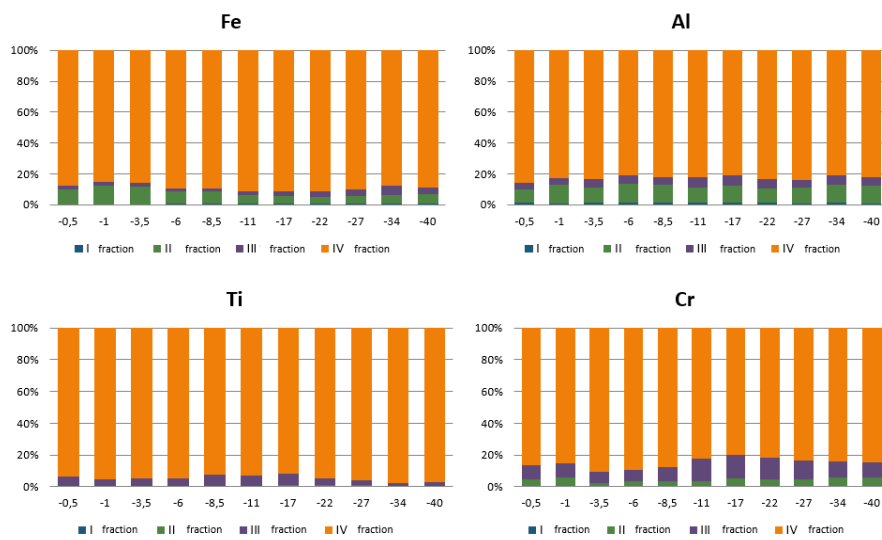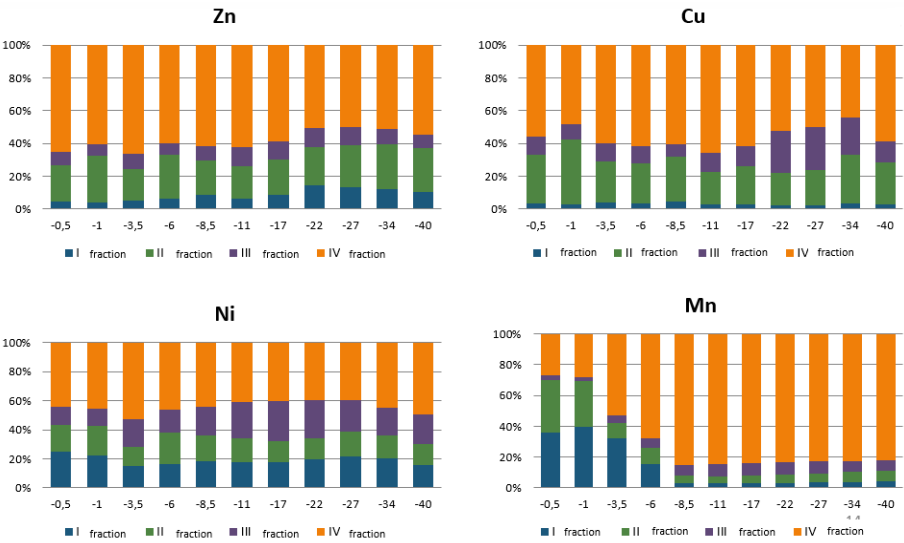
474　2017)

475

476

477

478   **Figure 2** – Fe, Al, Ti and Cr partitioning among the BCR fractions: labile (Fraction I), reducible

479   (Fraction II), oxidizable (Fraction III) and residual (total extracted minus the sum of the three

480   fractions, Fraction IV).

481

482

483

484

485

486

487

488

489

490 **Figure 3** – Zn, Cu, Ni and Mn partitioning among the BCR fractions: labile (Fraction I), reducible

491 (Fraction II), oxidizable (Fraction III) and residual (total extracted minus the sum of the three

492 fractions, Fraction IV).

493

494

495 **Figure 4** – Pb and Cd partitioning among the BCR fractions: labile (Fraction I), reducible (Fraction

496 II), oxidizable (Fraction III) and residual (total extracted minus the sum of the three fractions, Fraction

497 IV).
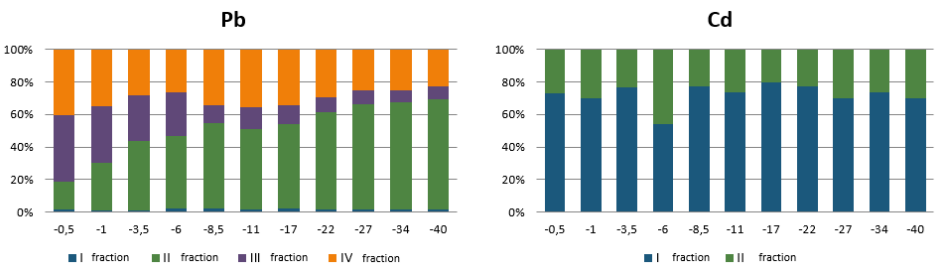
498

499

500 **Figure 5 –** Chemometric treatments on the total element content. *First panel*: bi-plot of scores and

501 loadings on PC1-PC2; *Second panel*: dendrogram obtained by HCA.
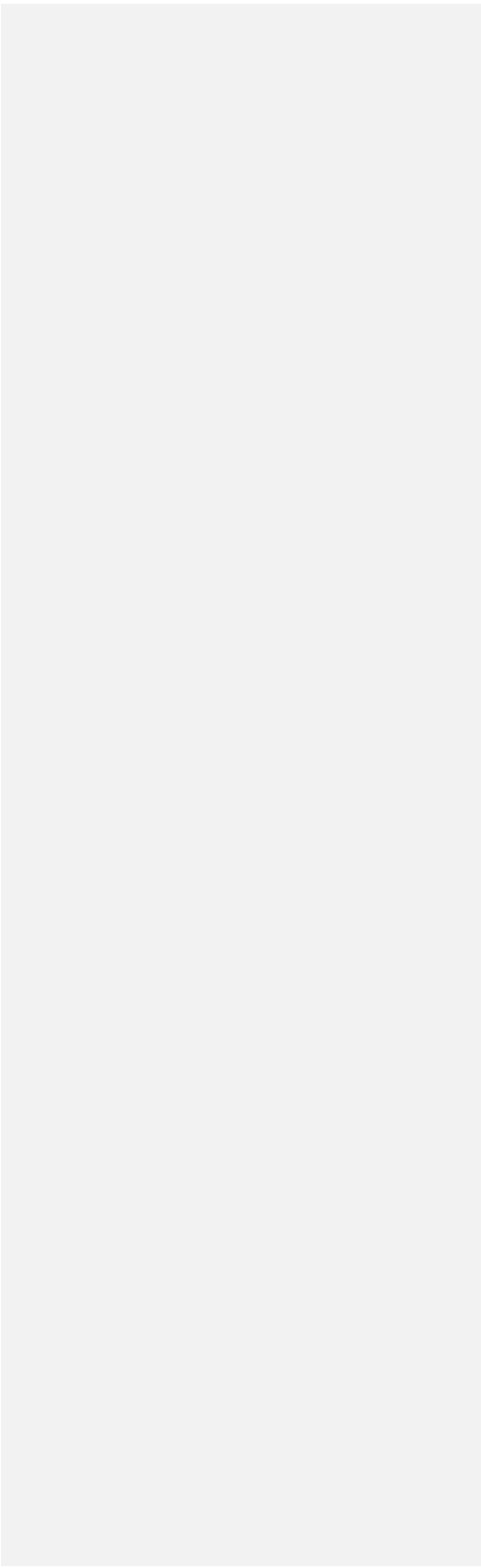
502

503
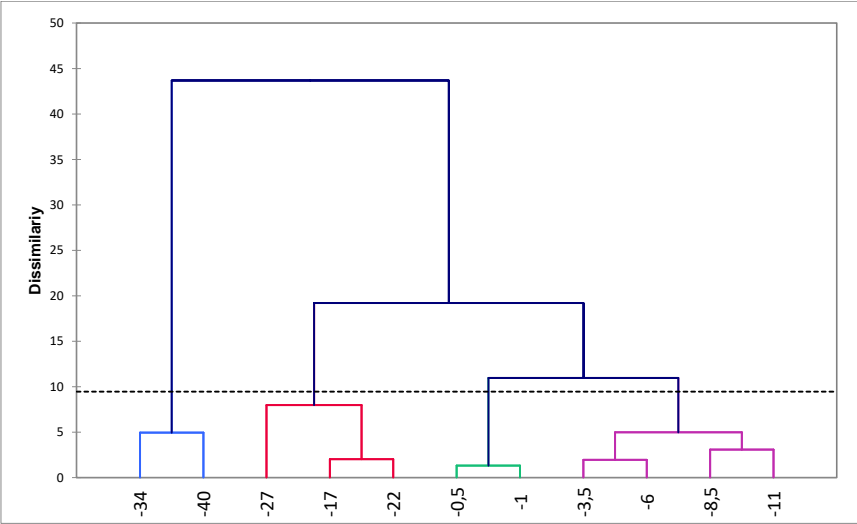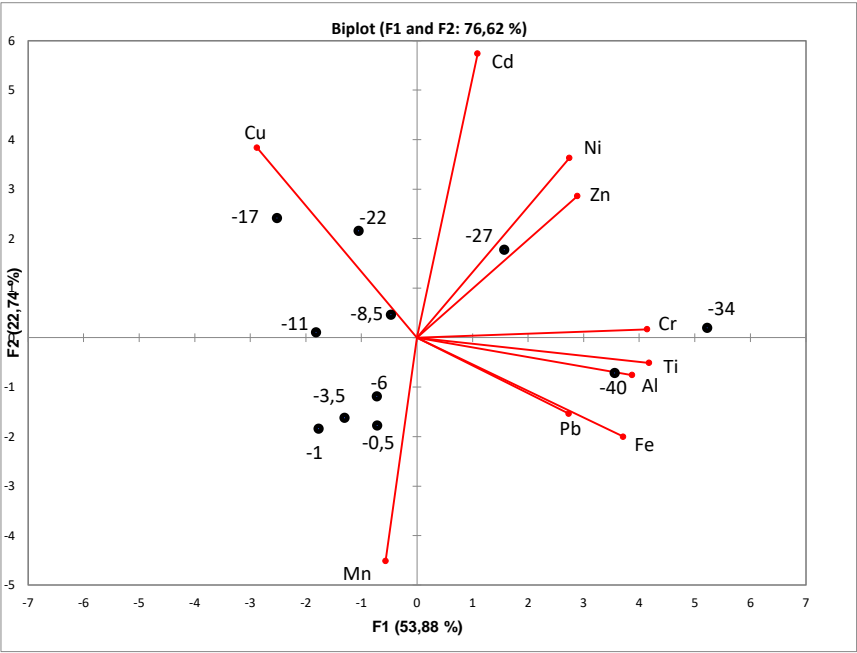
504

505

506

507

508

509   **References**

510   Abollino O, Giacomino A, Malandrino M, Mentasti E, Aceto M, Barberis R. Assessment of metal
511   availability in a contaminated soil by sequential extraction. Water, Air, and Soil Pollution
512   2006; 173: 315-338.
513   Arrigo KR, Van Dijken GL. Phytoplankton dynamics within 37 Antarctic coastal polynya systems.
514   Journal of Geophysical Research: Oceans 2003; 108.
515   Bacon JR, Davidson CM. Is there a future for sequential chemical extraction? Analyst 2008; 133: 25-
516   46.
517   Bergami C, Capotondi L, Langone L, Giglio F, Ravaioli M. Distribution of living planktonic
518   foraminifera in the Ross Sea and the Pacific sector of the Southern Ocean (Antarctica). Marine
519   Micropaleontology 2009; 73: 37-48.
520   Braguglia C, Campanella L, Petronio B, Scerbo R. Sedimentary humic acids in the continental margin
521   of the Ross Sea (Antarctica). International journal of environmental analytical chemistry
522   1995; 60: 61-70.
523   Calace N, Cremisini C, Galletti M, Mirante S, Petronio B. Copper and other trace elements strongly
524   bound to humic acids along sediment cores in the Ross Sea, Antarctica. Journal of
525   Environmental Monitoring 2005; 7: 1281-1286.
526   Calace N, Giglio F, Mirante S, Petronio BM, Ravaioli M. Sedimentary process inferences from humic
527   substances analysis and deposition rates (Western Ross Sea, Antarctica). International Journal
528   of Environmental Analytical Chemistry 2004; 84: 423-439.
529   Calvert S, Pedersen T. Sedimentary geochemistry of manganese; implications for the environment of
530   formation of manganiferous black shales. Economic Geology 1996; 91: 36-47.
531   Capodaglio G, Turetta C, Toscano G, Gambaro A, Scarponi G, Cescon P. Cadmium, lead and copper
532   complexation in antarctic coastal seawater. Evolution during the austral summer. International
533   journal of environmental analytical chemistry 1998; 71: 195-226.
534   Caroli S, Cescon P, Walton DWH. Environmental contamination in Antarctica: a challenge to
535   analytical chemistry: Gulf Professional Publishing, 2001.
536   Caroli S, Senofonte O, Caimi S, Robouch P, Pauwels J, Kramer G. Certified reference materials for
537   research in Antarctica: the case of marine sediment. Microchemical journal 1998; 59: 136-
538   143.
539   Casalino CE, Malandrino M, Giacomino A, Abollino O. Total and fractionation metal contents
540   obtained with sequential extraction procedures in a sediment core from Terra Nova Bay, West
541   Antarctica. Antarctic Science 2013; 25: 83-98.
542   Ciaralli L, Giordano R, Lombardi G, Beccaloni E, Sepe A, Costantini S. Antarctic marine sediments:
543   distribution of elements and textural characters. Microchemical Journal 1998; 59: 77-88.
544   Corradi N, Fierro G, Giordano F, Ivaldi R, Langone L, Pitta A. High-resolution seismic mapping of
545   the Holocene diatomaceous muddy drape in the Northern Joides Basin (Ross Sea, Antarctica).
546   Terra Antartica Reports 2003; 9: 83-88.
547   Cuong DT, Obbard JP. Metal speciation in coastal marine sediments from Singapore using a modified
548   BCR-sequential extraction procedure. Applied Geochemistry 2006; 21: 1335-1346.
549   DeMaster DJ, Dunbar RB, Gordon LI, Leventer AR, Morrison JM, Nelson DM, et al. Cycling and
550   accumulation of biogenic silica and organic matter in high-latitude environments: the Ross
551   Sea. Oceanography 1992; 5: 146-153.
552   DeMaster DJ, Ragueneau O, Nittrouer CA. Preservation efficiencies and accumulation rates for
553   biogenic silica and organic C, N, and P in high-latitude sediments: The Ross Sea. Journal of
554   Geophysical Research: Oceans 1996; 101: 18501-18518.
555   Domack EW, Taviani M, Rodriguez A. Recent sediment remolding on a deep shelf, Ross Sea:
556   implications for radiocarbon dating of Antarctic marine sediments. Quaternary Science
557   Reviews 1999; 18: 1445-1451.

Formattato: Italiano (Italia)

558 Duprat LP, Bigg GR, Wilton DJ. Enhanced Southern Ocean marine productivity due to fertilization
559   by giant icebergs. Nature Geoscience 2016; 9: 219.
560 Frignani M, Giglio F, Accornero A, Langone L, Ravaioli M. Sediment characteristics at selected sites
561   of the Ross Sea continental shelf: does the sedimentary record reflect water column fluxes?
562   Antarctic Science 2003; 15: 133-139.
563 Frignani M, Giglio F, Langone L, Ravaioli M, Mangini A. Late Pleistocene-Holocene sedimentary
564   fluxes of organic carbon and biogenic silica in the northwestern Ross Sea, Antarctica. Annals
565   of Glaciology 1998; 27: 697-703.
566 Froelich PN, Klinkhammer G, Bender ML, Luedtke N, Heath GR, Cullen D, et al. Early oxidation of
567   organic matter in pelagic sediments of the eastern equatorial Atlantic: suboxic diagenesis.
568   Geochimica et cosmochimica acta 1979; 43: 1075-1090.
569 Gleyzes C, Tellier S, Astruc M. Fractionation studies of trace elements in contaminated soils and
570   sediments: a review of sequential extraction procedures. TrAC Trends in Analytical
571   Chemistry 2002; 21: 451-467.
572 Greene CA, Gwyther DE, Blankenship DD. Antarctic mapping tools for MATLAB. Computers &
573   Geosciences 2017; 104: 151-157.
574 Hans Wedepohl K. The composition of the continental crust. Geochimica et Cosmochimica Acta
575   1995; 59: 1217-1232.
576 Hauck J, Gerdes D, Hillenbrand C-D, Hoppema M, Kuhn G, Nehrke G, et al. Distribution and
577   mineralogy of carbonate sediments on Antarctic shelves. Journal of Marine Systems 2012;
578   90: 77-87.
579 Heiri O, Lotter AF, Lemcke G. Loss on ignition as a method for estimating organic and carbonate
580   content in sediments: reproducibility and comparability of results. Journal of paleolimnology
581   2001; 25: 101-110.
582 Huckriede H, Meischner D. Origin and environment of manganese-rich sediments within black-shale
583   basins. Geochimica et Cosmochimica Acta 1996; 60: 1399-1413.
584 Ianni C, Magi E, Soggia F, Rivaro P, Frache R. Trace metal speciation in coastal and off-shore
585   sediments from Ross Sea (Antarctica). Microchemical Journal 2010; 96: 203-212.
586 Jickells T, An Z, Andersen KK, Baker A, Bergametti G, Brooks N, et al. Global iron connections
587   between desert dust, ocean biogeochemistry, and climate. science 2005; 308: 67-71.
588 Lambert F, Tagliabue A, Shaffer G, Lamy F, Winckler G, Farias L, et al. Dust fluxes and iron
589   fertilization in Holocene and Last Glacial Maximum climates. Geophysical Research Letters
590   2015; 42: 6014-6023.
591 Langone L, Frignani M, Labbrozzi L, Ravaioli M. Present-day biosiliceous sedimentation in the
592   northwestern Ross Sea, Antarctica. Journal of Marine Systems 1998; 17: 459-470.
593 Langone L, Frignani M, Ravaioli M, Bianchi C. Particle fluxes and biogeochemical processes in an
594   area influenced by seasonal retreat of the ice margin (northwestern Ross Sea, Antarctica).
595   Journal of Marine Systems 2000; 27: 221-234.
596 Lenz C, Behrends T, Jilbert T, Silveira M, Slomp CP. Redox-dependent changes in manganese
597   speciation in Baltic Sea sediments from the Holocene Thermal Maximum: An EXAFS,
598   XANES and LA-ICP-MS study. Chemical Geology 2014; 370: 49-57.
599 Malandrino M, Mentasti E, Giacomino A, Abollino O, Dinelli E, Sandrini S, et al. Temporal
600   variability and environmental availability of inorganic constituents in an Antarctic marine
601   sediment core from a polynya area in the Ross Sea. Toxicological & Environmental Chemistry
602   2010; 92: 453-475.
603 Martin JH, Fitzwater SE. Iron deficiency limits phytoplankton growth in the north-east Pacific
604   subarctic. Nature 1988; 331: 341.
605 Martin JH, Gordon RM, Fitzwater SE. Iron in Antarctic waters. Nature 1990; 345: 156.
606 Martínez-Garcia A, Rosell-Melé A, Jaccard SL, Geibert W, Sigman DM, Haug GH. Southern Ocean
607   dust–climate coupling over the past four million years. Nature 2011; 476: 312.

608   Merian E, Anke M, Ihnat M, Stoeppler M. Elements and their compounds in the environment:
609   occurrence, analysis and biological relevance: Wiley-VCH Verlag GmbH & Co. KGaA, 2004.
610   Mezgec K, Stenni B, Crosta X, Masson-Delmotte V, Baroni C, Braida M, et al. Holocene sea ice
611   variability driven by wind and polynya efficiency in the Ross Sea. Nature communications
612   2017; 8: 1-12.
613   Morel FM, Price N. The biogeochemical cycles of trace metals in the oceans. Science 2003; 300:
614   944-947.
615   Pedersen T, Price N. The geochemistry of manganese carbonate in Panama Basin sediments.
616   Geochimica et Cosmochimica Acta 1982; 46: 59-68.
617   Quevauviller P. Operationally defined extraction procedures for soil and sediment analysis I.
618   Standardization. TrAC Trends in Analytical Chemistry 1998; 17: 289-298.
619   Rauret G, López-Sánchez J-F, Sahuquillo A, Barahona E, Lachica M, Ure AM, et al. Application of
620   a modified BCR sequential extraction (three-step) procedure for the determination of
621   extractable trace metal contents in a sewage sludge amended soil reference material (CRM
622   483), complemented by a three-year stability study of acetic acid and EDTA extractable metal
623   content. Journal of Environmental Monitoring 2000; 2: 228-233.
624   Ravaioli M, Frignani M, Gambi M, Labbrozzi L, Langone L. Particle fluxes and sediment
625   characteristics at three selected sites in the Ross Sea (Antarctica). Oceanography of the Ross
626   Sea Antarctica. Springer, 1999, pp. 209-222.
627   Reddy KR, Xu CY, Chinthamreddy S. Assessment of electrokinetic removal of heavy metals from
628   soils by sequential extraction analysis. Journal of hazardous materials 2001; 84: 279-296.
629   Rhodes RH, Bertler NA, Baker JA, Sneed SB, Oerter H, Arrigo KR. Sea ice variability and primary
630   productivity in the Ross Sea, Antarctica, from methylsulphonate snow record. Geophysical
631   Research Letters 2009; 36.
632   Rivaro P, Messa R, Ianni C, Magi E, Budillon G. Distribution of total alkalinity and pH in the Ross
633   Sea (Antarctica) waters during austral summer 2008. Polar Research 2014; 33: 20403.
634   Salvi C, Salvi G, Stenni B, Brambati A. Palaeoproductivity in the Ross Sea, Antarctica, during the
635   last 15 kyr BP and its link with ice-core temperature proxies. Annals of Glaciology 2004; 39:
636   445-451.
637   Sedwick PN, DiTullio GR, Mackey DJ. Iron and manganese in the Ross Sea, Antarctica: seasonal
638   iron limitation in Antarctic shelf waters. Journal of Geophysical Research: Oceans 2000; 105:
639   11321-11336.
640   Smetacek V, Klaas C, Strass VH, Assmy P, Montresor M, Cisewski B, et al. Deep carbon export from
641   a Southern Ocean iron-fertilized diatom bloom. Nature 2012; 487: 313-319.
642   Tessier A, Campbell PG, Bisson M. Sequential extraction procedure for the speciation of particulate
643   trace metals. Analytical chemistry 1979; 51: 844-851.
644   Wersin P, Höhener P, Giovanoli R, Stumm W. Early diagenetic influences on iron transformations in
645   a freshwater lake sediment. Chemical Geology 1991; 90: 233-252.
646